IMAGE PROCESSING, PATTERN RECOGNITION

An efficient algorithm for overlapping bubbles segmentation

Afef Bettaieb [1], Nabila Filali [1], Taoufik Filali [1], Habib Ben Aissia [1]
[1] Laboratory of Metrology and Energetic Systems, National School of Engineers of Monastir, University of Monastir, Monastir, Tunisia

Abstract

Image processing is an effective method for characterizing various two-phase gas/liquid flow systems. However, bubbly flows at a high void fraction impose significant challenges such as diverse bubble shapes and sizes, large overlapping bubble clusters occurrence, as well as out-of-focus bubbles. This study describes an efficient multi-level image processing algorithm for highly overlapping bubbles recognition. The proposed approach performs mainly in three steps: overlapping bubbles classification, contour segmentation and arcs grouping for bubble reconstruction. In the first step, we classify bubbles in the image into a solitary bubble and overlapping bubbles. The purpose of the second step is overlapping bubbles segmentation. This step is performed in two subsequent steps: at first, we classify bubble clusters into touching and communicating bubbles. Then, the boundaries of communicating bubbles are split into segments based on concave point extraction. The last step in our algorithm addresses segments grouping to merge all contour segments that belong to the same bubble and circle/ellipse fitting to reconstruct the missing part of each bubble. An application of the proposed technique to computer generated and high-speed real air bubble images is used to assess our algorithm. The developed method provides an accurate and computationally effective way for overlapping bubbles segmentation. The accuracy rate of well segmented bubbles we achieved is greater than 90 % in all cases. Moreover, a computation time equal to 12 seconds for a typical image (1 Mpx, 150 overlapping bubbles) is reached.

Keywords: bubble images; highly overlapping bubbles; bubble recognition; image segmentation; digital image processing.

Citation: Bettaieb A, Filali N, Filali T, Ben Aissia H. An efficient algorithm for overlapping bubbles segmentation. Computer Optics 2020; 44(3): 363-374. DOI: 10.18287/2412-6179-CO-605.

Introduction

Precise measurement of bubbly flows is crucial to understand the bubble behavior, mass, and heat transfer pattern in various engineering processes. It also plays a vital role in advancing the development of the theoretical model in the two-phase flows study. Currently, numerous techniques can be used to measure bubbly flow that can be classified into two main groups, namely: intrusive and non-intrusive techniques. Typical intrusive techniques include conductivity probe [1, 2] and phase sensitive constant temperature anemometry [3]. Non-intrusive techniques include laser doppler anemometry [4], X-ray and ɣ-ray computed tomography [5, 6] and image processing techniques [7, 8]. Among these methods, high-speed imaging is an efficient, convenient and broadly used tool in the bubbly flow visualization and measurement. A diversity of information including bubble size, velocity and number density can be provided by the recorded images of bubbles [9 – 17].

However, the task of bubbles recognition in recorded image data is not easy. Diverse technical challenges will occur while using the image analysis methods. The flow around a rising bubble is complex. Due to the interaction between the dispersed and liquid phases, the behavior and shape of nearby bubbles may be affected. The surface of a bubble can be deformed and takes an irregular-shape if the bubble becomes unstable, or it is disturbed by the surrounding flow, or going through a process of coalescence / breakup. Also, bubbles overlap when the void fraction is more than 1 – 2 %. Two major challenging issues will be encountered when handling with images of a large cluster of overlapping bubbles: (1) how to accurately identify bubbles in the image and segment the detected boundaries into several curves; (2) how to correctly classify the separated curves that belong to the same bubble and reconstruct its missing parts.

Recently, many image processing techniques have been carried out to automatically analyze complex bubbly flow images. One way to deal with bubble clusters is to ignore them by constraint conditions such as the concavity index [18], or the sphericity / roundness [19]. However, in a recent study presented in [20] it was shown that even if the bubble clusters are assumed as a non-selective process, large bubbles are more likely to be present as clusters. Therefore, ignoring these clusters would bias the measurement and can introduce large uncertainty specially at higher void fractions. In other techniques, overlapping bubbles were approximated through an object recognition method which fits an ellipsoidal shape to the

object areas. Honkanen et al. in [21] proposed an original method to detect overlapping ellipsoidal bubbles in the dense bubbly flow. In their study, the connecting points of bubble cluster are extracted using the curvature-profile method. Then each cluster of bubble arcs is fitted by an ellipse to reconstruct the missing parts. However, the technique used for segments grouping often suffers from inaccuracy even in the case of the small bubbles cluster. Moreover, it is computationally expensive.

Other authors have focused upon segmenting bubbles exploiting watershed algorithm [22], break point approach [23] and Hough transform method [24]. The Hough transform is suitable for detecting circular bubbles as shown in [25, 26]. A good accuracy was shown for small spherical shape bubbles or solid spheres. Honkanen et al. in [27] used the break point technique to separate boundaries of overlapping bubbles. The un-occluded edges of individual bubbles were obtained by this method. Lau et al. in [28] proposed an image processing technique that classifies the detected objects into a solitary bubble and overlapping bubbles. The watershed algorithm is applied in a second step to segment the overlapped bubbles. Nevertheless, the watershed algorithm suffers from over-segmentation and under-segmentation, especially when dealing with complex bubble shape. These errors are quantified in Lau et al. [28] study, but solutions to overcome those challenges are not suggested. The watershed combined with a set of morphological operations are used in the study of [29] to separate large bubble clusters consisting of various sizes. This method minimizes the risk of over-segmentation often encountered with the watershed algorithm. Also, the drawbacks of the watershed method are solved in a recent study developed by Villegas et al. [30]. This algorithm is devoted to the identification of ellipsoidal overlapping bubbles in the dense bubbly flow. To separate the overlapped bubbles, a combination of previous algorithms presented in [21, 28] with the watershed technique is used.

A new approach to recognize overlapping elliptical shape bubbles is presented in [31]. For contour segmentation, the dominant points are detected exploiting the polygonal approximation algorithm. Then, the candidate segments are grouped based on an average distance deviation (ADD) criterion and two constraints. However, these constraints are empirically determined and must be adjusted for each image of overlapping bubbles.

Fu et al. in [32] proposed a robust technique that combines optical, geometrical and topological information to segment and reconstruct the overlapping bubbles in higher void fraction conditions. The clustered bubbles boundaries are divided into separated arcs exploiting boundary curvature and image intensities. Then, a topology analysis that combines watershed algorithm, adaptive threshold and bubble skeleton is used to regroup arcs that belong to the same bubble. Finally, the ellipse fitting technique with the inner bubble information are exploited to reconstruct the missing parts of each individual bubble. The results show that the proposed method can accurately measure the bubbly flows at a void fraction up to 18 %. More recently, a robust approach to analyze complex images of large overlapping bubble clusters is proposed in [33]. In this study, Langlard et al. provided an automated technique called global segment detection (GSC) and sub-clustering process to group the edge segments that belong to the same bubble. Their approach is both efficient in terms of ellipsoidal bubble detection and in terms of computing performance due to the parallelization potential offered by the sub-clustering process.

Overall, these techniques remain limited regarding their robustness to analyze large overlapped bubble clusters in dense bubbly flows. Moreover, the processing of a large size/number of images and the online monitoring of bubbly flows require significant improvements in computation speed of algorithms. This motivated us to research a more valuable approach both in terms of results accuracy and computation time, to efficiently analyze high void fraction bubble flow images.

This paper seeks to address the aforementioned challenges. In this study, we introduce a fully automated technique for the recognition of spherical/ellipsoidal highly overlapping bubbles.

The remainder of this paper is structured as follows: a description of the proposed algorithm is given in the first Section. Experimental results obtained with our method and comparisons with those of the state of the art are shown in Section 2. Finally, conclusions are given in the last Section.

1. Methodology description

The basic outline of the proposed approach for overlapping spherical / ellipsoidal bubbles segmentation and reconstruction is described in brief in Fig. 1. Starting from a gray level image, the recognition process is carried out in three main steps:

1) splitting the image into regions of interest (ROI) which either contain an individual bubble or a cluster of bubbles;
2) contour segmentation of overlapped bubbles and
3) arcs grouping for bubble shape reconstruction.

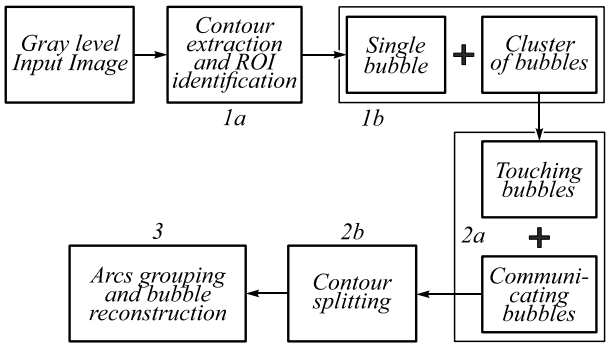

Fig. 1. Image processing sequences for overlapped bubbles recognition

1.1. Bubbles classification

Given a gray level image as input, our recognition process starts with building an image edge map and ROI identification in order to classify bubbles into single bubble and bubble cluster.

Generally, most of the algorithms discussed above starts by detecting edges of bubbles, and then uses the edge map for further high-level processing. Most of traditional edge detection operators use preprocessing approaches such as filtering to remove noise and a threshold to low-level feature extraction. Nevertheless, there are several drawbacks in the performance of these techniques. The performance of thresholding approaches is limited by the bubble size, noise, as well as the intensities difference between the bubble and the background. Minimizing noise by filtering operations results in blurred and distorted boundaries. Moreover, the performance of these detectors depends significantly on the shape of the object. The authors in [34] showed that their detection efficiency decreased to around 54 % in the case of a circular object. Due to these difficulties, preprocessing step must be applied so as to not distort or suppress the signal of interest, and the most effective solution is to adopt an approach that completely prevents the preprocessing step. In this study an accurate edge detection algorithm performing in real-time developed by the authors is used. This technique is based on the exploitation of raw images in order to preserve all features details until the final phase of treatment. The principle of this detector is described in [35].

The outline of each closed object is presented in two forms: a vector consisting of the coordinates of all contour pixels and a set of edge segments building based on a polygon approximation technique described in [36], each consisting of a linear and contiguous pixel chain. The set of segments will be used later in the rest of the algorithm in order to accelerate the computation time. Fig. 2 illustrates an example of the edge detection results.

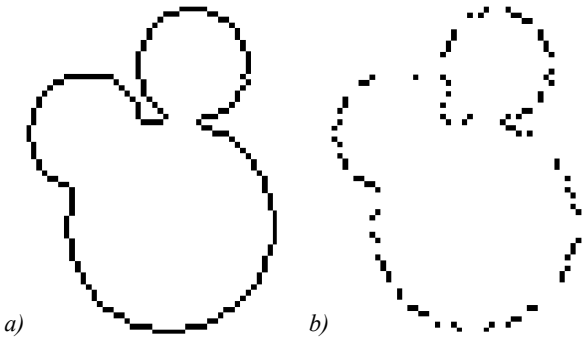

a) *b)*

Fig. 2. Bubbles contours detection results: a) conventional edge map, b) the set of edge segments

Then, the contour image is split into small image patches containing either a solitary bubble or an overlapping bubble cluster. Each ROI is presented by its corresponding bounding box and its label.

Once extracted ROI are available, an identification step is carried out to determine whether this ROI contains an individual bubble or a bubble cluster. Since the bubbles studied in this work have a circular shape, the single bubbles are defined by a roundness factor computation. The roundness is determined using the following formula:

$$\psi = \frac{4\pi A}{S^2}. \quad (1)$$

With A is the object area and S its perimeter. Note that a circular bubble has a roundness of unity.

However, adopting the roundness criterion only to detect overlapping bubbles has some obvious drawbacks. For example, in the study of Lau et al. [28] an image patch is defined as a solitary bubble if the roundness factor is < 1.25. This predefined threshold makes their approach not fully automatic, since it cannot be applied in a general case. Also, in some cases, a bubbles cluster ROI may have a roundness of unity like a single bubble.

In order to avoid misclassification and achieving an automatic recognition process, all ROIs which have a unit roundness are further processed with the Euclidean Distance Transform (EDT) operator [37]. An ROI is classified as a single bubble image if it has a single local maximum. The roundness computation combined with the DT ensure an accurate and automatic classification of bubbles images.

1.2. Segmentation of overlapping bubbles

After classification, the second step is to separate the boundaries of overlapping bubbles. This step is performed in two subsequent operations:

1) classification of overlapping bubbles ROI into touching bubbles and communicating bubbles and
2) contour splitting of communicating bubbles based on a concavity analysis.

Classification of overlapping bubbles ROIs

An example of overlapping bubbles ROI obtained from the previous step is illustrated by Fig. 3. We can clearly see that an image patch may contain either touching bubbles in just one point (Fig. 3*a*) or a completely overlapping bubbles that we have named communicating bubbles (Fig. 3*b*).

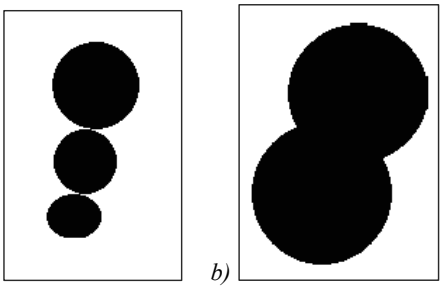

a) *b)*

Fig. 3. Examples of overlapped bubbles ROI: (a) three touching bubbles and (b) two communicating bubbles

In order to distinguish these patches, the edge pixels of each ROI are arranged in anticlockwise direction starting from the leftmost point. An edge pixel is defined as a contact point if its coordinates are repeated twice in the list. If

none contact point is found, the ROI will be defined as communicating bubbles. Otherwise, this ROI will be defined as touching bubbles. An example of results for 3 touching bubbles is illustrated by the following Fig. 4.

The number of single bubbles in a touching bubbles ROI is the local maximum number in its Euclidean Distance Transform (EDT) [37].

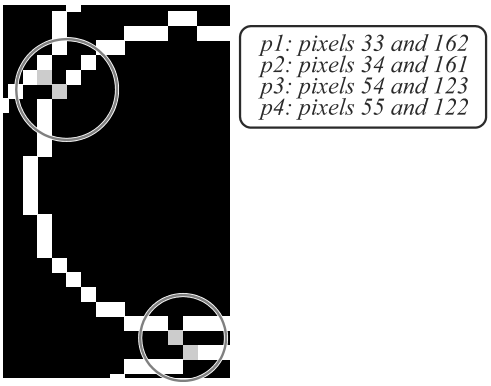

Fig. 4. Example of 3 touching bubbles detection process

Contour splitting of communicating bubbles

As mentioned above, a concavity analysis will be performed in this study to separate overlapping bubbles. The concavity-based techniques consider outlines and shapes of objects to detect separate points instead of gray level intensities. Currently, numerous classical techniques can be exploited to detect concave points such as dominant points detection by polygonal approximation technique [38], the detection of local minima in the curvature function [39], extracting the maximum curvature points from the concave region of the contour based on the definition of convexity and a sliding variable size rectangular window [40], or using corner points and an area ratio of a circular mask [41], and so on. However, most of these techniques suffer from considerable computations, inaccuracy and are not suited to the segmentation of a large number of overlapping bubbles. In order to overcome the aforementioned challenges, a method based on angle feature and a linear correlation coefficient to detect concave points is proposed in this study.

To reduce the calculation time, the degree of concavity is measured between edge segments extracted in the first step of our algorithm. Hence, the total number of points exploited to calculate concaveness value is decreased. Then, the computation time will be decreased.

Given a set of edge segments,

$$E = \left\{ s_i \left(ps_i, pe_i \right) \mid i = 1, 2, ..., n \right\},$$

where n is the number of edge segments and s_i is the ith segment on the contour with a start and end points ps_i and pe_i, respectively. The concavity of a candidate point p_i on the boundary is measured as follows:

$$\alpha(p_i) = \angle ps_i\, pe_i\, pe_{i+1}, \tag{2}$$

where $p_i = pe_i = ps_{i+1}$ (the end point of a segment is the start point of the next segment).

A point p_i is qualified as concave if it meets both the following criteria:

(1) $\alpha(p_i) < \alpha_{th}$ (α_{th} is a threshold angle obtained from training phase and it was set to 130°).

(2) the line $\overline{ps_i\, pe_{i+1}}$ does not reside inside the bubbles.

The second criteria is used to avoid misjudgment. Although a point p_i has a large concavity, it may not be located in the real concave area. The second rule guarantees that only a real concave point is selected.

However, as shown in Fig. 5, concave points can be divided into two main kinds: obvious and unobvious points. Obvious points can be easily detected by angle feature due to its sharply gradient change (Fig. 5*a*). While, the curvature change in the case of an unobvious point is small (Fig. 5*b*). It is hard to detect it by angle proprieties only.

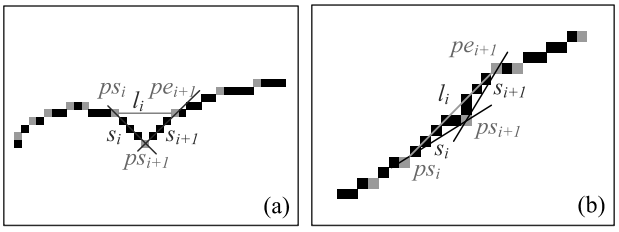

Fig. 5. Concave points detection: (a) obvious points detection and (b) unobvious points detection

Thus, to measure the slope change of s_i and s_{i+1}, a linear correlation coefficient of the point (p_i) is computed as follows:

$$\begin{aligned} \mathrm{corr}(p_i) &= \frac{E[(x-\mu_x)(y-\mu_y)]}{\sigma_x \sigma_y} = \\ &= \frac{\sum_{k=-1}^{1} (x_{i+k} - \bar{x})(y_{i+k} - \bar{y})}{\sqrt{\sum_{k=-1}^{1} (x_{i+k} - \bar{x})^2} \sqrt{\sum_{k=-1}^{1} (y_{i+k} - \bar{y})^2}}, \end{aligned} \tag{3}$$

where (x_i, y_i) are the coordinates of the point p_i and $(\bar{x}, \bar{y})$ are the mean values of ps_i, p_i and pe_{i+1}.

$$-1 \le \mathrm{corr}(p_i) \le 1.$$

There is a high possibility that the 3 points (ps_i, p_i and ps_{i+1}) are on the same line when $|\mathrm{corr}(p_i)|$ approaches 1. A point p_i is classified as concave if it satisfies the following two rules:

(1) $|\mathrm{corr}(p_i)| > \mathrm{corr}_{th}$ (where corr_{th} is a coefficient threshold obtained from training phase. Experimentally, it is set to 0.97).

(2) $\overline{s_i s_{i+1}} > \mathrm{dis}_{th}$ (where $\overline{s_i s_{i+1}}$ is the distance between ps_i and pe_{i+1} and dis_{th} is a distance threshold obtained from training phase. Experimentally, it is set to 6).

The first constraint is easy to fill. When the 3 points are closed, so distance criterion is applied. This constraint

will decrease the concave point detection error caused by the noise or the small turn produced by digitization.

By combining these two methods, the accuracy of concave points detection in a cluster of overlapping bubbles is significantly improved. Fig. 6 illustrates an example of using the proposed outline segmentation approach to separate the overlapped bubbles boundaries. The concave points detected by the angle proprieties only are highlighted by squares. The concave points detected by both methods are highlighted by lozenges.

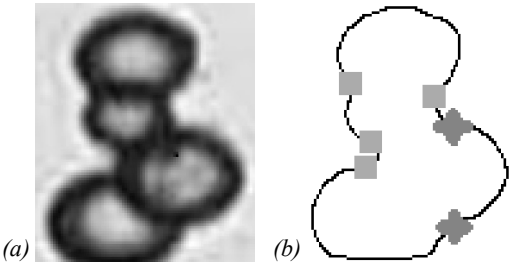

Fig. 6. Example of concave point extraction result: a) original image, b) concave points extraction: the squares are obvious concave points and the lozenges are unobvious concave points

Following the concave points detection, we now split the contour into n segments (where n is the total number of concave points) by every two adjacent points on it in the anticlockwise direction. Each segment is assumed to belong at least to one bubble embedded in the cluster, and a bubble can potentially include several segments. As a consequence, it is mandatory to find the best combination of n segments into m bubbles in order to extract the most probable cluster decomposition.

1.3. Arcs grouping and bubbles reconstruction

The next step in our algorithm addresses arcs grouping to merge all contour arcs that belong to the same bubble and circle/ellipse fitting to reconstruct the missing part of each bubble.

Bubbles boundaries are split into a set of contour arcs by concave points denoted $\{a_1, a_2, ..., a_n\}$, where n is the number of arcs. a_i is the contour arc limited by concave points c_i and c_{i+1}. a_i is connected with a_{i-1} and a_{i+1}. To reduce the computation time, two cases are discussed according to the total number of concave points *nc*:

If $2 \le nc \le 3$, contours are split into 2 or 3 arcs. Any two arcs are linked by a concave point. Hence, grouping process is not needed and each contour arc is fitted to circle/ellipse directly.

If $nc > 3$, $\{a_1, a_2, \ldots a_n\}$ are classified into groups by arcs grouping rules.

In this paper, we introduce an efficient method for bubble arcs grouping inspired from the EDcircles algorithm [42]. This method is chosen due to its ability to produce a high accurate result in real-time. Given a set of contour arcs, the algorithm performs into two main steps: (1) joining the arcs into circle/ellipse candidates and (2) validating these candidates based on the Helmholtz principle.

In order to reduce the computation time and enhance the efficiency of our method; we have established a set of possible arcs that may be joined together before starting the arcs grouping process. Based on the basic rule of contour arcs grouping, two neighborhood arcs that are linked and split by one concave point should not be set into the same group. Thus, the grouping rules are applied only to non-neighboring arcs. Therefore, the number of candidate arcs in the grouping process will be decreased. Then, the computation time will be also reduced.

Arcs grouping

Fig. 7 shows the flowchart of the main steps of this method.

The idea is to look for arcs with similar radii and nearby centers, and to establish a list of candidate arcs that may belong to the same bubble. Given an arc a_i to be joined with a candidate arc a_j, two scenarios are possible: spherical bubble detection and elliptical bubble detection.

In the two cases, the following two criterions must be satisfied:

(1) Radius difference constraint: the difference of radius between a_i and the candidate arc a_j must be within a predefined threshold.

(2) Center distance constraint: the distance between the centers of a_i and a_j must be within a predefined threshold.

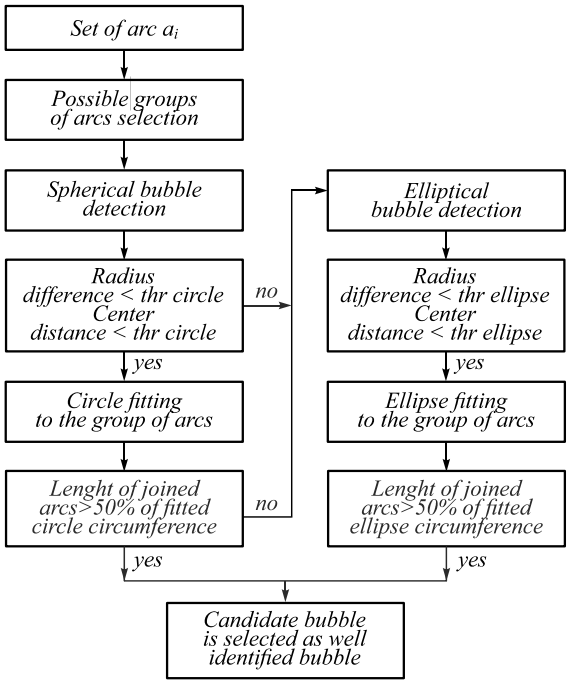

Fig. 7. Flowchart of the arcs grouping scheme

The least squares fitting algorithm is used to find the radius and the centers of the arcs. The threshold values must not exceed 25% of a_i's radius for the case of a circle and 50% of a_i's radius for an ellipse. As an example, in the case of a spherical bubble searching, if a_i's radius is 100, then all possible arcs whose radii are between 75 and

125 and their centers are within 25 pixels of a_i's center would be taken as candidates for arc join.

Once the candidate arcs have been selected, the subsequent step is to join them one by one with the arc a_i by fitting a circle/ellipse to the pixels making up these arcs using the least squares circle fit algorithm or direct least square fitting of ellipses. Then we decide if the fitted circle/ellipse is taken as a candidate bubble. Thus, the ratio between the total number of pixels of the joined arcs and the circumference of the fitted circle/ellipse is computed. If this ratio is greater than 50 %, the fitted circle/ellipse is taken as a candidate else it is rejected.

The following fig. 8 shows an example of using the above flowchart to determine bubble number in a cluster of four overlapping bubbles. With the contour splitting algorithm described above, the cluster boundary is divided into four arcs. These arcs are first grouped into two possible groups based on the basic rule of contour segments grouping mentioned above: group 1 (arc 1 + arc 3) and group 2 (arc 2 + arc 4). Then, the two grouping rules (radius and centers constraints) are verified for the two candidate groups. In the first group arc 3 is selected as a candidate to be joined with arc 1. Arc 3 satisfy the radius constraint ((r 1 – r 3) < (r 1/4); r 1 and r 4 represent arc 1 and arc 3 radius, respectively), but fails the center constraint ((c 1 – c 3) > (r 1/4); c 1 and c 3 represent arc 1 and arc 3 centers, respectively). So, these two arcs will not be joined together and each arc will be considered as a separated bubble and it will be fitted by a circle/ellipse to reconstruct the missing parts. In the second group arc 4 is selected as a candidate to be joined with arc 2. Arc 4 satisfy both radius and centers constraints. Thus, the two arcs will be joined together and fitted by an ellipse to reconstruct the missing part. At this stage, the four arcs are matched to three candidate bubbles. The last step is decision if these bubbles are well identified or not. Thus, the ratio between the length of joined arcs and the circumference of the fitted circle/ellipse is computed. If it is greater than 50 %, then the fitted circle/ellipse is taken as well identified bubble else it will be rejected.

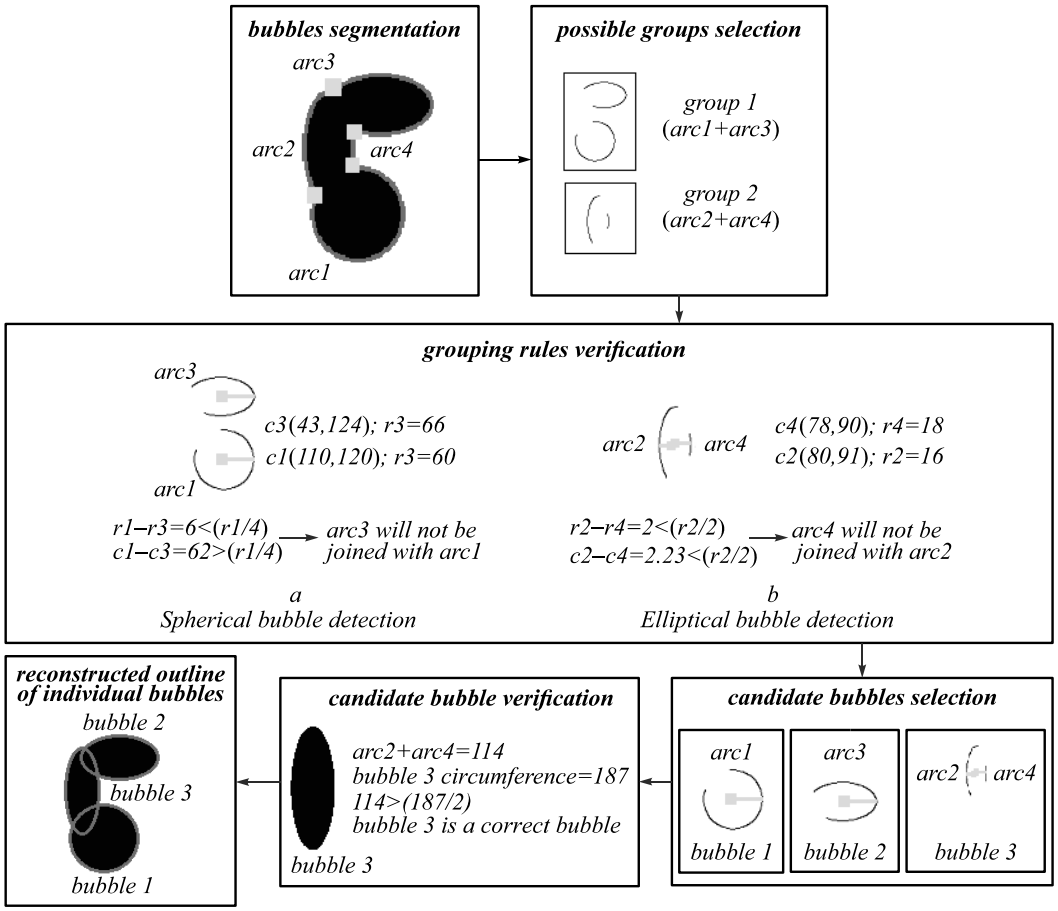

Fig. 8. Arcs grouping and bubbles reconstruction process

Circle/ellipse validation by Helmholtz principle

Just because many arcs can be gathered in circles/ellipses does not imply that all candidates are valid selections. Thus, as a last step, a validation algorithm based on the Helmholtz principle is used to remove invalid selections and return only the valid ones. The basic idea is to calculate the level orientation field of an image and search a contiguous set of pixels with similar line orientation. The alignment between a pixel and a circle is defined by the adaptation of the alignment between a pixel and a segment proposed in [42]. A point (p_i) on the boundary of a given circle/ellipse is aligned with it if (p_i) is aligned with the tangent (T) to the

circle/ellipse at that point. Thus, the angle (p_i) and angle (T) must be within $p\times\pi$ degrees with each other if (p_i) and the circle/ellipse are aligned with a precision p.

Once all aligned points are detected the NFA (number of false alarms) of a circle/ellipse having n points as length and k aligned pixels is computed as follows:

$$NFA(n,k) = N^5 \sum_{i=k}^{n} \binom{n}{i} p^i (1-p)^{n-i}, \quad (4)$$

where N^5 is the number of potential circles/ellipses in an $N\times N$ image. The circle/ellipse is accepted as valid if $\mathrm{NFA}(n,k)\le\varepsilon$; otherwise, it is rejected. The epsilon (ε) was set to 1, which corresponds to a single false detection by image.

2. Experimental results and analysis

In order to assess the efficiency of the proposed method, both synthetic and real bubble images were investigated. In this study, the bubble recognition algorithm runs on a computer equipped with an Intel® Core ™ i7-3770 CPU performing at 3.4 GHZ and 16 GB RAM. For the implementation of the code, we used the VS2015 configured with OpenCV 3.0.0.

2.1. Recognition of synthetic images

To quantify the performance of the recognition bubble approach, we first implement our algorithm to synthetic images of bubbles. Indeed, the number of bubbles involved in an image is perfectly known and each bubble is fully characterized, which is not the case for real bubbles images.For this purpose, a set of 50 synthetic images of 100–150 overlapping circular and elliptical bubbles was considered. The semi-minor and semi-major axis (denoted a and b, respectively) of the bubble follow a uniform law in the intervals [5, 15] and [10, 40] pixels, respectively.

Fig. 9 shows an example of the results of our recognition method for an image of this dataset including both single and overlapping bubbles. Fig. 9*a* and 9*b* illustrates the original image and the ground truth regions of all bubbles constructed manually, respectively. Fig. 9*c* and 9*d* shows the results of the first step (ROI extraction and bubbles classification), Fig. 9*e* exhibits the concave point extraction result and Fig. 9*f* illustrates the bubbles segmentation obtained with our proposed method. The bubbles contours are superimposed on the original image. From this figure, it can be seen that all connecting points are extracted efficiently by our approach (Fig. 9*e*). Obvious (squares) and unobvious (lozenges) concave points can be accurately extracted using the method proposed in Section.1.2. Satisfactory result for unobvious concave points extraction can be obtained by the proposed method. Also, it is obvious that all bubbles are segmented and reconstructed accurately.

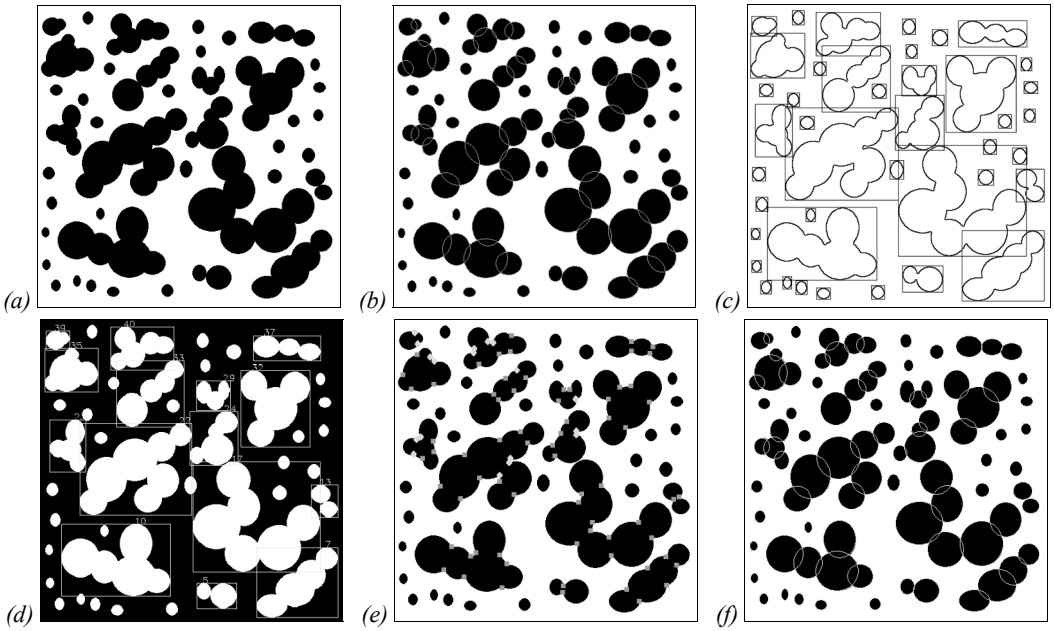

Fig. 9. Segmentation result on a synthetic image: (a) original image, (b) ground truth, (c) edge detection and ROI extraction, (d) bubbles classification, (e) concave points detection and (f) result of segmentation

In order to assess the recognition quality of bubbles with different degrees of overlapping, the dataset of images was categorized into three groups: low, medium and high. The images of low overlapping degree are characterized by a slight touch among the bubbles. Most bubbles overlap in the case of medium overlapping degree. In the high degree case, bubbles overlap more severely. The efficiency of the proposed approach was compared with two methods pulled from the state of the art: the technique proposed by Zafari et al. [43] and the one proposed by Park et al. [44]. For the sake of illustration, an example of the results of the recognition process with the three techniques applied on three images from the dataset considered here are compared in Fig. 10.

In these samples, it is clear that all the bubble clusters are mostly well resolved with our algorithm in all images.

All the bubbles are correctly identified and reconstructed in the case of low and medium degrees of overlapping versus 95.34 % in the case of high degree. On the other hand, as illustrated in Fig. 10*a* and 10*b*, the two techniques from the literature are unable to detect precisely all bubbles, especially when a large cluster of bubbles is processed: 83.7 % of bubbles are well identified with Zafari's method versus 76.74 % with park's technique.

To further evaluate the accuracy of the proposed method, it was quantitatively compared with the above-mentioned algorithms [43, 44]. Three quantitative measures metrics were exploited. The first is the percentage of accurate segmented bubbles (PA). The second represents the probability of over-segmented bubbles (PO), which estimates the percentage of a bubble that is segmented into several bubbles by the algorithm. The third is the probability of under-segmented bubbles (PU), which represents the number of un-detected bubbles. The mean values of the three metrics obtained with the three techniques for the set of images considered in this study are tabularized in Table 1. The adjustable parameters values of the two literature techniques were fixed according to the author's recommendations.

As shown in Table 1, our approach outperforms both Zafari's method and Park's method. The accuracy is improved by 6.61 % compared with Zafari's algorithm and it is improved by 18.18 % with respect to park's technique. The main error of our algorithm is under-detection in very high overlapped bubbles images. The two other methods suffer from both over-segmentation and under-segmentation. The Zafari's method performs better than Park's method in all groups of images. By comparing the three metrics values, we can conclude that our algorithm is more efficient than the other two techniques.

Table 1. Comparison of performances of three algorithms

Method	PA (%)	PO (%)	PU (%)
Zafari et al. [43]	91.74	3.3	4.96
Park et al. [44]	80.17	11.57	8.26
Our method	98.35	0	1.65

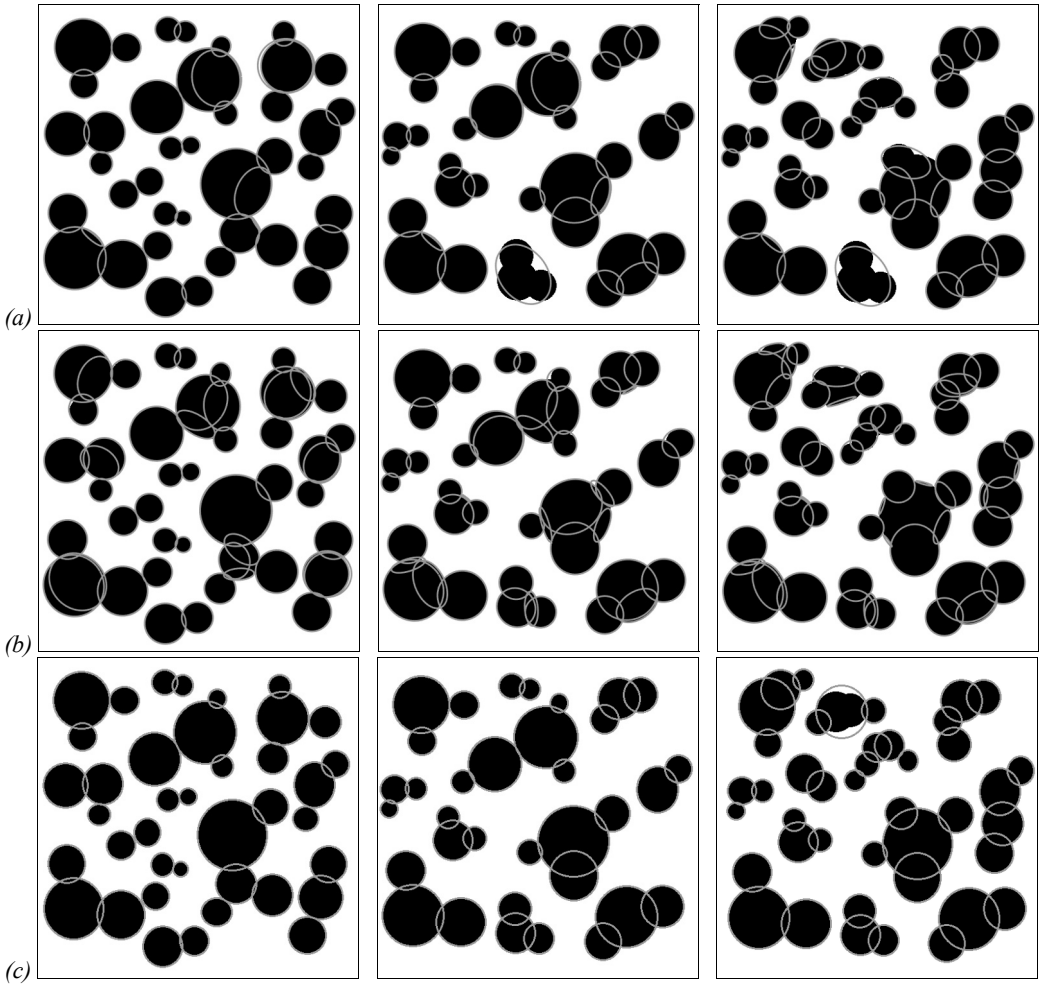

Fig. 10. Example of recognition results on a 3 synthetic images with different degrees of overlapping; the left column: low degree, the middle column: medium degree and the right column: high degree; (a) Zafari et al. [43], (b) Park et al. [44] and (c) our algorithm

2.2. Recognition of real bubbly flow images

In addition to the satisfied results achieved on the computer-generated images, our recognition algorithm was applied to identify the different bubbles on a set of experimental images of gas/liquid flow taken from [45].

An example of the obtained result is illustrated in Fig. 11. From visual observation, it is obvious that all bubbles were identified accurately.

Another example of the bubble identification result is shown in Fig. 12. This image exhibits a high ratio of bubble clusters (70 overlapped bubbles). The agreement between the detected circles/ellipses and the bubble boundaries is very good, 67 correct detected bubbles versus only 3 bad detections (marked by boxes), so proving the technique efficiency on real bubbly flow images.

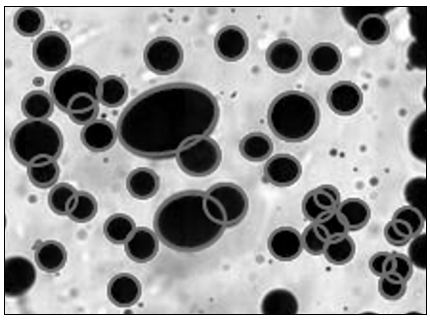

Fig. 11. Performances of our method on an experimental image: the bubble contours are superimposed on the original image. The bubble on the image border is not considered

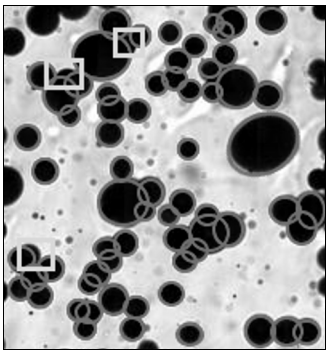

Fig. 12. Another example of our method results. 67 bubbles have been well detected. The boxes highlight the three bad detections. The bubble on the image border is not considered

Generally, two cases of bad recognition are observed. The first case occurs when the bubble cluster shape is very complex, so some concave points may be missed. In addition, the shape of the bubbles has a significant deviation from a circle or an ellipse, which is not the scope of this study. The second one concerns bubbles with blurred contours.

Also, the efficiency of the proposed method was quantitatively compared with the technique proposed by Zafari et al. [43]. The total number of bubbles in 5 samples and the number of the bubbles correctly identified by each of techniques in comparison are tabularized in Table 2.

Overall, our proposed algorithm is the best performer for all images. Fig. 13 illustrates one exemplary result of the recognition process performed by our approach and the competing technique. This figure is an example of multiple bubble clusters. As we can see, the proposed technique identifies most of the touched bubbles in this image where Zafari's method suffers from under-segmentation. From 131 bubbles included in this image, our method gives 118 bubbles well detected and separated versus only 73 detected by Zafari's algorithm. Due to the fact that there are wide and strongly overlapped bubble clusters, the competing method fails to identify each single bubble included in this image. This underperformance compared to our approach is mainly due to the concave point detection algorithm exploited by Zafari et al. [43]. In their study, the concave points are detected based only on the features of angular and concavity. This method fails to give satisfactory concave points, especially in the case of blurry bubbles or highly overlapped bubble clusters.

Table 2. Rate of well segmented bubble in terms of total number of bubbles

Samples	Total # of bubbles	Total # of the correctly identified bubbles		Percentage %	
		Our method	Zafari [43]	Our method	Zafari [43]
Image 1	53	53	46	100	86.79
Image 2	93	87	80	93.54	86.02
Image 3	131	118	73	90.07	55.72
Image 4	150	143	122	95.33	81.33
Image 5	200	192	138	96	69

Fig. 14*a* and 14*b* shows the results of concave points detection by our algorithm and Zafari's method, respectively, for the same image shown in Fig. 13. It is observed that in the case of many touching bubbles (surrounded by boxes in Fig. 14), Zafari's method failed to detect all concave points especially unobvious one. Due to the little change of the concavity, it is hard to detect them with the concavity rules only.

However, the proposed concave point detection algorithm is more effective and stable. There are fewer undetected or inaccurately detected concave points with our algorithm, which is evident by comparing Fig. 14*a* and 14*b*. As shown in Fig. 14*a*, most of obvious concave points are well detected and they lie at the turn of the bubble edge. Satisfactory unobvious concave point detection result can be obtained by the proposed algorithm (represented by lozenges in Fig. 14*a*). In addition, our method requires less computation time as the total number of points exploited to calculate concaveness value is decreased.

Otherwise, the computation times of our algorithm and Zafari's method running on the computer abovementioned were measured for an image size in the inter-

val [64 Kpx, 1 Mpx]. It was found that the average execution time per image ranged from 8 to 22 s and from 4 to 12 s with Zafari's algorithm and the proposed technique, respectively. These results revealed that our method is computationally efficient. Moreover, computation time could be significantly decreased by the parallelization of the algorithm over Multiprocessor and/or GPUs.

To summarize, these comparison results allow us to conclude that our algorithm is more stable and efficient than the other methods, for both synthetic and real images.

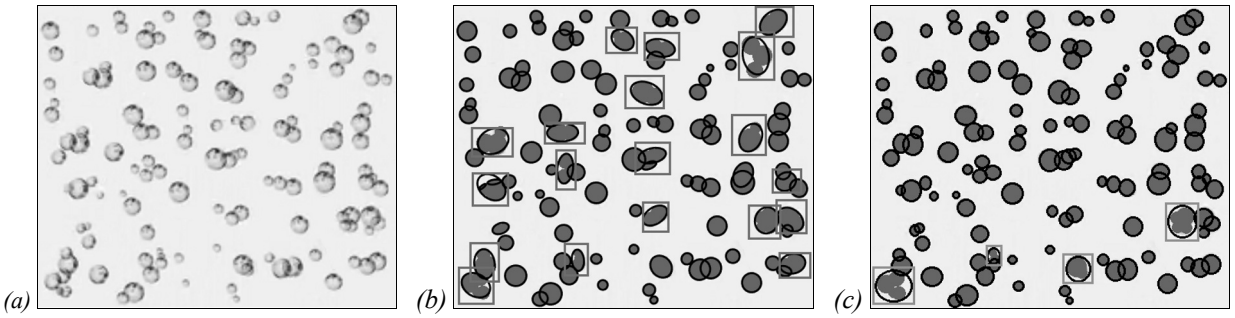

Fig. 13. Performance comparison: (a) original image, (b) Zafari's method and (c) our method. The boxes highlight the bad detections (the colors are inverted due to printing issues)

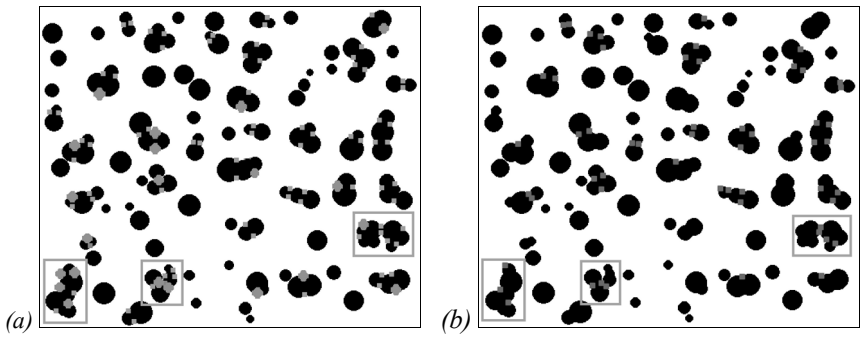

Fig. 14. Concave points detection performance comparison: (a) our method (the squares are obvious concave points and the lozenges are unobvious concave points) and (b) Zafari's algorithm

Conclusion

A new multi-level approach to segment and reconstruct highly overlapped bubbles is proposed in this paper. In the first step, the proposed method classifies the images patches of overlapped bubbles into touching and communicating bubbles. This step remarkably reduces the computation time since the rest of the algorithm will be applied to the overlapping bubbles only. Then, the communicating bubbles patches are passed through a segmentation process in order to separate clusters into edge segments based on a concavity analysis. An effective method for obvious and unobvious concave points detection is introduced to guarantee accuracy of our algorithm. The last step addresses grouping of different segments that belong to the same bubble and circle/ellipse fitting to reconstruct the bubble shape.

The proposed method was first validated using synthetic images. A further assessment is performed by comparing our algorithm to two techniques from the state of the art. This comparison has highlighted significant enhancements: 98 % of the segmented bubbles were correct for the proposed algorithm compared to the proportion of 80 % (respectively 91 %) for the one of Park et al. [44] (resp. Zafari et al. [43]).

An application of the proposed technique to high-speed real air bubble images has highlighted the ability of this approach to resolve highly overlapped bubble clusters.

Last but not the least, our approach is computationally efficient. For example, the average execution time for a typical image (1 Mpx, 150 overlapping bubbles) is about 12 seconds on an Intel® Core ™ i7-3770 CPU.

Due to its ability to be parallelized, computational time can be significantly reduced by parallelization on GPU (the graphic processing units), thus opening up perspectives for real time monitoring of two-phase flow processes in a wide range of industrial applications. Future work will focus also on the analysis, 3D reconstruction and tracking of more complex shape of the bubble (when the bubble does not exhibit a spherical or elliptical shape but a more irregular shape).

References

[1] Wang D, Song K, Fu Y, Liu Y. Integration of conductivity probe with optical and X-ray imaging systems for local air–water two-phase flow measurement. Meas Sci Technol 2018; 29(10): 105301.

[2] Wang D, Liu Y, Talley JD. Numerical evaluation of the uncertainty of double-sensor conductivity probe for bubbly flow measurement. Int J Multiph Flow 2018; 107: 51-66.

[3] Mercado JM, Gmez DC, Gils DV, Sun C, Lohse D. On bubble clustering and energy spectra in pseudo-turbulence. J Fluid Mech 2010; 650: 287-306.

[4] Ristic SS, Ilic JT, Cantrak DS, Ristic OR, Jankovic NZ. Estimation of laser-Doppler anemometry measuring volume displacement in cylindrical pipe flow. Thermal Science 2012; 16(4): 1027-1042.

[5] Song K, Liu Y. A compact X-ray system for two-phase flow measurement. Meas Sci Technol 2018; 29(2): 025305.
[6] Bieberle A, Härting H-U, Rabha S, Schubert M, Hampel U. Gamma-ray computed tomography for imaging of multiphase flows. Chemie Ingenieur Technik 2013; 85(7): 1002-1011. DOI: 10.1002/cite.201200250.
[7] Bouche E, Roig V, Risso F, Billet AM. Homogeneous swarm of high-Reynolds-number bubbles rising within a thin gap. Part 1. Bubble dynamics. J Fluid Mech 2012; 704: 211-231.
[8] Bouche E, Roig V, Risso F, Billet A-M. Homogeneous swarm of high-Reynolds-number bubbles rising within a thin gap. Part 2. Liquid dynamics. J Fluid Mech 2014; 758: 508-521.
[9] Fu Y, Liu Y. 3D bubble reconstruction using multiple cameras and space carving method. Meas Sci Technol 2018; 29(7): 075206.
[10] Cerqueira RFL, Paladino EE, Ynumaru BK, Maliska CR. Image processing techniques for the measurement of two-phase flow bubbly pipe flow using particle image and tracking velocimetry (PIV/PTV). Chem Eng Sci 2018; 189: 1-23.
[11] Yan X, Jia Y, Wang L, Cao Y. Drag coefficient fluctuation prediction of a single bubble rising in water. Chem Eng J 2017; 316: 553-562.
[12] Wang H, He X, Vishwanath P, Xiao-Zhi G. A Novel one-camera-five-mirror three-dimensional imaging method for reconstructing the cavitation bubble cluster in a water hydraulic valve haihang. Appl Sci 2018; 8(10): 1783.
[13] Zhao L, Sun L, Mo Z, Tang J, Hu L, Bao J. An investigation on bubble motion in liquid flowing through a rectangular Venturi channel. Experimental Thermal and Fluid Science 2018; 97: 48-58.
[14] Xue T, Xu LS, Zhang SZ. Bubble behavior characteristics based on virtual binocular stereo vision. Optoelectronics Letters 2018; 14(1): 44-47.
[15] Zhao L, Mo Z, Sun L, Xie G, Liu H, Du M, Tang J. A visualized study of the motion of individual bubbles in a venturi type bubble generator. Progress in Nuclear Energy 2017; 97: 74-89.
[16] Zhong S, Zou X, Zhang Z, Tian H. A flexible image analysis method for measuring bubble parameters, Chem Eng Sci 2016; 141: 143-153.
[17] Besbes S, El Hajem M, Ben Aissia H, Champagne JY. PIV measurements and Eulerian-Lagrangian simulations of the unsteady gas-liquid flow in a needle sparger rectangular Bubble column. Chem Eng Sci 2015; 126: 560-572.
[18] Mena PC, Pons MN, Teixeira JA, Rocha FA. Using image analysis in the study of multiphase gas absorption. Chem Eng Sci 2005; 60: 5144-5150.
[19] Bailey M, Gomez CO, Finch JA. Development and application of an image analysis method for wide bubble size distributions. Miner Eng 2005; 18: 1214-1221.
[20] Kracht W, Emery X, Paredes C. Astochastic approach for measuring bubble size distribution via image analysis. Int J Miner 2013; 121: 6-11.
[21] Honkanen M, Saarenrinne P, Stoor T, Niinimaki J. Recognition of highly overlapping ellipse-like bubble images. Meas Sci Technol 2005; 16: 1760-1770.
[22] Bleau A, Leon LJ. Watershed-based segmentation and region merging. Comput Vis Image Underst 2000; 77: 317-370.
[23] Teh CH, Chin RT. On the detection of dominant points on digital curves. IEEE Trans Pattern Anal Mach Intell 1989; 11: 859-872.
[24] Pei SC, Horng JH. Circular arc detection based on Hough transform. Patt Recogn Lett 1995; 16: 615-625.
[25] Mathai V, Prakash VN, Brons J, Sun C, Lohse D. Wake-driven dynamics of finite-sized buoyant spheres in turbulence. Phys Rev Lett 2015; 115: 124501.
[26] Prakash VN, Tagawa Y, Calzavarini E, Mercado JM, Toschi F, Lohse D, Sun C. How gravity and size affect the acceleration statistics of bubbles in turbulence. New J Phys 2012; 14: 105017.
[27] Honkanen M. Reconstruction of a three-dimensional bubble surface from high-speed orthogonal imaging of dilute bubbly flow. WIT Trans Eng Sci 2009; 63: 469-480.
[28] Lau YM, Deen NG, Kuipers JAM. Development of an image measurement technique for size distribution in dense bubbly flows. Chem Eng Sci 2013; 94: 20-29.
[29] Karn A, Ellis C, Arndt R, Hong J. An integrative image measurement technique for dense bubbly flows with a wide size distribution. Chem Eng Sci 2015; 122: 240-249.
[30] Villegas LR, Colombet D, Guiraud P, Legendre D, Cazinac S, Cockx A. Image processing for the experimental investigation of dense dispersed flows: application to bubbly flows. Int J Multiphase Flow 2019; 111: 16-30.
[31] Zhang WH, Jiang X, Liu YM. A method for recognizing overlapping elliptical bubbles in bubble image. Pattern Recogn Lett 2012; 33(12): 1543-1548.
[32] Fu Y, Liu Y. Development of a robust image processing technique for bubbly flow measurement in a narrow rectangular channel. Int J Multiphase Flow 2016; 84: 217-228.
[33] Langlard M, Al-Saddik H, Charton S, Debayle J. An efficiency improved recognition algorithm for highly overlapping ellipses: application to dense bubbly flows. Pattern Recogn Lett 2018; 101: 88-95.
[34] Liu X, Fang S. A convenient and robust edge detection method based on ant colony optimization. Opt Commun 2015; 353: 147-157.
[35] Bettaieb A, Filali N, Filali T, Ben Aissia H. GPU acceleration of edge detection algorithm based on local variance and integral image: application to air bubbles boundaries extraction. Computer Optics 2019; 43(3): 446-454. DOI: 10.18287/2412-6179-2019-43-3-446-454.
[36] Parvez MT, Mahmoud SA. Polygonal approximation of digital planar curves through adaptive optimizations. Pattern Recogn Lett 2010; 13: 1997-2005.
[37] Man D, Uda K, Ito Y, Nakano K. Accelerating computation of Euclidean distance map using the GPU with efficient memory access. Int J Paral Emergent Distrib Sys 2013; 28: 383-406.
[38] Zhang WH, Jiang X, Liu YM. A method for recognizing overlapping elliptical bubbles in bubble image. Pattern Recogn Lett 2012; 33: 1543-1548.
[39] Altheimer M, Häfeli R, Wälchli C, von Rohr PR. Shadow imaging in bubbly gas-liquid two-phase flow in porous structures. Exp Fluids 2015; 56(9): 177.
[40] Farhan M, Yli-Harja O, Niemistö A. A novel method for splitting clumps of convex object incorporating image intensity and using rectangular window-based concavity point pair search. Pattern Recogn 2013; 46: 741-751.
[41] Wencheng Wang, Xiaohui Yuan. Seperating touching particles: A concavity-based method using the area ratio of a circular mask. IEEE Systems, Man, and Cybernetics Magazine 2018; 4(2): 24-32.
[42] Akinlar C, Topal C. ED Circles: A real-time circle detector with a false detection control. Pattern Recogn 2013; 46: 725-740.
[43] Zafari S, Eerola T, Sampo J, Kälviäinen H, Haario H. Segmentation of partially overlapping nanoparticles using concave points, International Symposium on Visual Computing. ISVC 2015: Advances in Visual Computing 2015: 187-197.
[44] Park C, Huang JZ, Ji JX, Ding Y. Segmentation, inference and classification of partially overlapping nanoparticles. IEEE Trans Pattern Anal Mach Intell 2013; 35(3): 669-681.

[45] Langlard M. La géométrie aléatoire pour la caractérisation 3D de populations denses de particules : application aux écoulements diphasiques. PhD thesis. University of Lyon 2019.

Author's informations

Afef Bettaieb graduated from National School of Engineers of Monastir, Tunisia in 2013, achieving M.D. in Electronics and Telecommunications. She is a PHD student in Electrical department at the National School of Engineers of Monastir, Tunisia, since 2014. Her research interests are image processing and computer vision techniques, real time image processing, parallel programming and GPU programming language. E-mail: *bettaiebafef@gmail.com* .

Nabila Filali received the Engineering degree in Electrical Engineering from the National School of Engineers of Monastir (ENIM), Tunisia in 1989 and the Advanced Studies Diploma in 1992 from the University of Tunis and Ph.D. degree in Image Processing and Embedded Electronic systems at the University of Monastir, Tunisia and the University of Jean Monnet - Saint Etienne, France in 2009. She is a Research professor in Electrical department at ENIM, where she teaches courses in Computer Vision and Image Processing, High Speed Networks and NoC, New Technologies and Advanced Architectures of Microprocessors and Multiprocessors. Her current research interests include embedded system implementation, GPU computing and real time image processing. E-mail: *merchaoui.filali@laposte.net* .

Taoufik Filali is a Research Professor in Electrical department at the National School of Engineers of Monastir, Tunisia since 1982. His interests include embedded system implementation, GPU computing and image processing. He received his Ph.D. degree in Image, Vision and Signal at the University of Jean Monnet – Saint Etienne, France in 2011. He is interested in research projects related to the application of metrology and image processing techniques within the field of fluid dynamics, real time processing and medical domain and many industrial projects.
E-mail: *tafilali@laposte.net* .

Habib Ben Aissia received the Engineers Doctor energetic from a high school in France in 1986 (ENSMA at Poitiers). He is a full Professor at the National School of Engineers of Monastir, Energetic Engineering department, Director of the Laboratory of Metrology and Energetic Systems (LR18ES21). He is author of about 80 articles. He is one by the founding members of National School of Engineers of Monastir. E-mail: *habib.benaissia@enim.rnu.tn* .

Received July 17, 2019. The final version – October 25, 2019.